Evaluation of Spatio-Temporal Variogram Models for Mapping Xco$_2$ Using Satellite Observations: A Case Study in China

Lijie Guo, Liping Lei, Zhao-Cheng Zeng, Pengfei Zou, Da Liu, and Bing Zhang, *Senior Member, IEEE*

Abstract—Greenhouse Gases Observing Satellite (GOSAT), which measures column-averaged carbon dioxide dry air mole fractions (Xco$_2$) from space, provides new data sources to improve our understanding of carbon cycle. The available GOSAT data, however, have many gaps and are irregularly positioned, which make it difficult to directly interpret their scientific significance without further data analysis. Spatio-temporal geostatistical prediction approach can be used to fill the gaps for global and regional Xco$_2$ mapping. It is important to choose a suitable spatio-temporal variogram model since modeling spatio-temporal correlation structure using variogram model is a critical step in the geostatistical prediction. In this study, three different flexible spatio-temporal variogram models, including the product-sum model, Cressie–Huang model, and Gneiting model, are used to model the spatio-temporal correlation structure of Xco$_2$ over China, using the Atmospheric CO$_2$ Observations from Space retrievals of the GOSAT (ACOS-GOSAT) Xco$_2$ (v3.3) data products. The three models are compared and evaluated using the weighted mean square errors (WMSE) indicating the fitness between the empirical variogram surface and the theoretical variogram model, cross-validation for quantifying prediction accuracies, and the performance of the three models when used to fill the spatial gaps and generate Xco$_2$ maps in 3-day temporal interval. The results indicate that 1) the model fitness of the commonly used product-sum model is slightly better than Cressie–Huang model and Gneiting model as indicated from WMSE, and 2) all the three models present similar summary statistics in cross-validation, all with a significantly high correlation coefficient of 0.92, and about 83% of prediction error within 2 ppm and about 53% within 1 ppm, and (3) differences between the mapping results using the three models are generally less than 0.1 ppm, and no significant differences can be identified. As a conclusion from the above results, all the three variogram models can precisely catch the empirical characteristics of the spatio-temporal correlation structure of Xco$_2$ over China, and the precision and effectiveness of predicting and mapping Xco$_2$ using the three models are almost the same.

Index Terms—ACOS-GOSAT, carbon dioxide, mapping, spatio-temporal kriging, spatio-temporal variogram models.

I. Introduction

COLUMN-AVERAGED carbon dioxide dry air mole fractions (Xco$_2$) from the Greenhouse gas Observation Satellite (GOSAT) [1], [2] launched in 2009 has become new data sources to improve our understanding of carbon sources and sinks [3], [4]. The Xco$_2$ data retrieved from GOSAT, however, have many gaps and are irregularly positioned due to the influences of the clouds and the satellite orbit configurations [5]. Such data cannot well demonstrate the comprehensive continuous variations of CO$_2$ in space and time, which makes it difficult to directly interpret the spatial and temporal characteristics of atmospheric CO$_2$ concentrations [6]. To address the problem, both spatial-only and spatio-temporal geostatistical approach has been applied to fill the gaps [7]–[9]. The correlation structure modeling, including the choice of variogram model and the estimation of the model parameters, is the most critical step in the geostatistical approach [10]. It is, therefore, important to choose a suitable variogram model by taking the characteristics and behavior of the model into account [11]. The spatio-temporal geostatistics using spatio-temporal variogram was adopted for mapping satellite-observed Xco$_2$ [12] because Xco$_2$ distribution presents both nonconstant spatial trend and a temporal trend including seasonal cycle and yearly trend [13]. To model the spatio-temporal empirical variogram, exploratory analysis of the marginal spatial and temporal variogram of Xco$_2$ will be conducted. The spatial-only geostatistical prediction approach will not be discussed in this paper since the temporal structures, such as seasonal effect, in the Xco$_2$ data are ignored in the approach [7], [14]–[16].

Statistical modeling using geostatistics for analyzing the spatio-temporal process that evolves in space and time is of great interest in many areas of application, including the environmental sciences [17], climate prediction and meteorology [18]–[20], biology [21], hydrology [22], and medicine [23], [24]. Spatio-temporal geostatistical modeling depends strongly

L. Guo, P. Zou, and D. Liu are with the Key Laboratory of Digital Earth Science, Institute of Remote Sensing and Digital Earth, Chinese Academy of Sciences, Beijing 100094, China, and also with the University of Chinese Academy of Sciences, Beijing 100049, China (e-mail: guolijie12@gmail.com; zoupengfei90@126.com; liuda@radi.ac.cn).

Z.-C. Zeng was with the Key Laboratory of Digital Earth Science, Institute of Remote Sensing and Digital Earth, Chinese Academy of Sciences, Beijing 100094, China. He is now with the Institute of Space and Earth Information Science, The Chinese University of Hong Kong, Shatin 999077, Hong Kong (e-mail: zzhaoch@gmail.com).

L. Lei and B. Zhang are with the Key Laboratory of Digital Earth Science, Institute of Remote Sensing and Digital Earth, Chinese Academy of Sciences, Beijing 100094, China (e-mail: lplei@ceode.ac.cn; zb@ceode.ac.cn).

Color versions of one or more of the figures in this paper are available online at http://ieeexplore.ieee.org.

Digital Object Identifier 10.1109/JSTARS.2014.2363019

on the choice of the covariance model for characterizing the spatio-temporal correlation structure. Therefore, there are many recent advances in developing spatio-temporal variograms and covariance models to meet the demand for modeling space–time data [25], [26]. Among them, large efforts have been focused on the development of nonseparable spatio-temporal variograms and covariance models that are able to model the space–time interactions in the environmental and geophysical processes. A diverse range of models of nonseparable spatio-temporal autocorrelation structures in spatio-temporal geostatistics are proposed in the literature [18], [20], [26]–[29]. Among them, the three models, including the product-sum model [27], Cressie–Huang model [20], and Gneiting model [18], are the most commonly used and extensively studied spatio-temporal variogram models [19], [30], [31]. Cressie–Huang model is a class of nonseparable covariance functions constructed using a systematic way based on spectral approach [20], whereas Gneiting model is constructed using an approach extended from Cressie–Huang model and provides a general classes of valid spatio-temporal covariance functions [18]. The product-sum model, on the other hand, is a class of covariance functions constructed using a convex combination of two separated spatial and temporal covariance functions [26] and it is, therefore, flexible and easy to implement [30]. Several studies have been conducted to compare and evaluate different spatio-temporal covariance models to investigate their effectiveness and limits in specific case studies [19], [22], [24], [30]–[32]. De Iaco *et al.* [30], [32] applied the spatio-temporal geostatistics to daily ozone data and hourly NO_2 data and found that the product-sum model works the best comparing to Cressie–Huang and Gneiting models. Martínez-Ruiz *et al.* [24] also preferred the product-sum model when assessing the mortality risk in Spain. In the study of runoff and precipitation, Skøien *et al.* [22] showed that the product-sum model is a slightly better fit than Cressie–Huang model. From Huang *et al.* [31], Cressie–Huang model, however, showed the best behavior among the other models when analyzing the solar radiation data. It can be found from these previous studies that the suitable spatio-temporal covariance model varies from case to case. For the modeling of atmospheric greenhouse gases, Zeng *et al.* [12] developed a gap-filling approach for the GOSAT data using the product-sum model to obtain spatio-temporal Xco_2 predictions. However, no attempts have been made to investigate the best covariance model for spatio-temporal geostatistical analysis of the Xco_2 datasets from satellite observations. Modeling the space–time interaction of atmospheric Xco_2 with suitable covariance functions can better characterize and predict the spatio-temporal variation of Xco_2. Therefore, a comparative study and evaluation of different spatio-temporal covariance models for satellite Xco_2 data is of great importance.

In this paper, the modeling of the spatio-temporal correlation structure of Xco_2 using different spatio-temporal variogram models for mapping will be evaluated and compared in the study area over mainland China. The variogram models to be evaluated include three typical spatio-temporal variogram models, the product-sum model, Cressie–Huang model, and Gneiting model. The spatio-temporal trend, including the spatial trend and seasonal effect, of the satellite-observed Xco_2

data will be firstly analyzed and quantified. The Xco_2 data are then detrended to generate the residual for further variogram modeling study. The performance of the three spatio-temporal variogram models for mapping will be evaluated in the following three aspects, including 1) the weighted mean square errors (WMSE) for comparing the fitness of the theoretical variogram models to the empirical variogram calculated from data, 2) the commonly used summary statistics in cross-validation, which will be defined in Section III-E, for comparing the prediction accuracies of geostatistical prediction using different variogram models, and 3) comparison of the mapping results with the three spatio-temporal variogram models and the corresponding kriging variance indicating the prediction uncertainty. The objective of this paper is to explore the best variogram models, which is, on one hand, flexible and effective enough to quantify the characteristics of spatio-temporal correlation structure of atmospheric Xco_2, and, on the other hand, provides the best prediction precision in mapping using spatio-temporal kriging. In the Section II, we give a description of the data used in this paper. In Section III, we introduce the basic theories of the methodologies used, including spatio-temporal variogram modeling, space–time kriging prediction, and cross-validation technique for evaluating model precision. Section IV presents the results and discussion, and the conclusion follows in Section V.

II. DATA

In this study, we collected GOSAT Xco_2 data products released by the Atmospheric CO_2 Observations from Space (ACOS) project in v3.3 over China land region spanning from April 2009 to July 2012. GOSAT, launched on January 23, 2009, has been observing the reflected sun-light spectra from space by the thermal and near-infrared sensor for carbon observation Fourier transform spectrometer (TANSO-FTS) to retrieve the concentrations of carbon dioxide and methane, the two major greenhouse gases [2], [33]. The ACOS project applied the approaches including the calibration, validation, and retrieval algorithms which are developed for orbiting carbon observatory (OCO) to the GOSAT's calibrated spectra measurements (Level 1B) and generated the ACOS-GOSAT Xco_2 dataset [34]–[36]. The ACOS-GOSAT Xco_2 data include the glint ocean data, land high gain data, and land medium data [37]. Only the land high gain data are used, by the recommendation from the ACOS Level 2 Standard Product Data User's Guide, v3.3 [37]. The data is first screened using the advanced screening criteria described in the user guide to limit the retrievals to those which have the highest confidence [37], and then the global biases are removed by applying the bias correction approach introduced in the data user guide [37]. This screened and bias-corrected ACOS v3.3 Xco_2 data are used in the following analysis.

Fig. 1 shows the spatial distribution of the used dataset. We take 3 days as a calculating time unit as the GOSAT orbiting period is 3 days, in which the temporal variability of Xco_2 is relatively small and, therefore, not considered [13]. In general there are nearly 122 time units in 1 year ($365/3 \approx 122$), and from June 2009 to May 2012, 366 time units of ACOS-GOSAT data were used in this study.
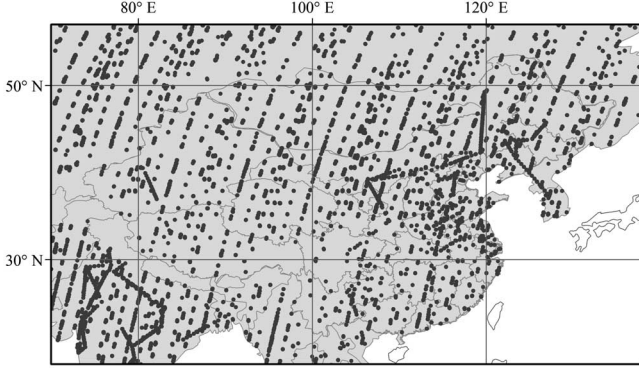
Fig. 1. Spatial distribution of used ACOS-GOSAT v3.3 data (black dots) from June 2009 to May 2012 across study area (gray color).

III. METHODOLOGY

A. Spatio-Temporal Random Field Formalism

We model the GOSAT Xco_2 data as a partial realization of a spatio-temporal random function $Z = Z\{Z(\boldsymbol{s}, t), (\boldsymbol{s}, t) \in D \times T\}$ where $D \in \boldsymbol{R}^2$ and $T \in \boldsymbol{R}$ [38]. As described in the World Meteorological Organization report [13], atmospheric CO_2 presents both a nonconstant spatial trend and a temporal trend, including the seasonal cycle and yearly trend. Therefore, the spatio-temporal random function can be decomposed into a mean component and a residual component, given by

$$Z(\boldsymbol{s}, t) = m(\boldsymbol{s}, t) + R(\boldsymbol{s}, t) \quad (1)$$

where the mean component $m(\boldsymbol{s}, t)$ is a deterministic mean model in space and time and the residual component $R(\boldsymbol{s}, t)$ is assumed to be an intrinsically stationary random field [38], [39]. In this study, the deterministic spatio-temporal mean component $m(\boldsymbol{s}, t)$ is further decomposed into a spatial trend $m_1(\boldsymbol{s})$ and temporal trend $m_2(t)$, i.e., $m(\boldsymbol{s}, t) = m_1(\boldsymbol{s}) + m_2(t)$, as described in [25]. The estimated spatio-temporal mean component is then subtracted from the full dataset to yield the spatio-temporal residuals component $R(\boldsymbol{s}, t)$, and will be used in the following analysis.

B. Spatio-Temporal Empirical Variogram

Application of spatio-temporal geostatistical approach to prediction and mapping of satellite-observed Xco_2 includes the analysis of spatial-temporal correlation structure of regional variables using the spatio-temporal variogram [38], and the optimal prediction of Xco_2 value at an unsampled location and time [10]. Spatio-temporal empirical variogram [27], [39] is calculated from the residual component $R(\boldsymbol{s}, t)$. The empirical variogram value $\hat{\gamma}_{ST}(\boldsymbol{r}_s, r_t)$ at the lag $(\boldsymbol{r}_s, r_t)$ is given by

$$\hat{\gamma}_{ST}(\boldsymbol{r}_s, r_t) = \frac{1}{2 |I(\boldsymbol{r}_s, r_t)|}$$
$$\times \sum_{I(\boldsymbol{r}_s, r_t)} [R(\boldsymbol{s} + \boldsymbol{h}_s, t + h_t) - R(\boldsymbol{s}, t)]^2 \quad (2)$$

where $\boldsymbol{h}_s \in \mathrm{D}$, $h_t \in \mathrm{T}$, and $|I(\boldsymbol{r}_s, r_t)|$ are the cardinality of the set $|I(\boldsymbol{r}_s, r_t)| = \{(\boldsymbol{s} + \boldsymbol{h}_s, t + h_t) \in \mathrm{H}, (\boldsymbol{s}, t) \in \mathrm{H}$ such that $\|\boldsymbol{r}_s - \boldsymbol{h}_s\| < \delta_s \wedge \|r_t - h_t\| < \delta_t\}$. (δ_s, δ_t) is the spatial tolerance and temporal tolerance. The spatial empirical marginal variogram $\hat{\gamma}_{ST}(\boldsymbol{r}_s, 0)$ is denoted as $\hat{\gamma}_S(\boldsymbol{r}_s)$, and the temporal empirical marginal variogram $\hat{\gamma}_{ST}(\boldsymbol{0}, r_t)$ is denoted as $\hat{\gamma}_T(r_t)$.

C. Marginal and Spatio-Temporal Variogram Modeling

Due to the convex property of both the spatial and the temporal marginal variograms, as shown in Section IV, the commonly used exponential model for modeling convex variogram was used and fit the two marginal variograms in space and time. The chosen exponential model is given by

$$\gamma(h; \theta) = \begin{cases} 0, & h = 0 \\ N + C \cdot (1 - \exp(-\|h\|/a)), & h \neq 0 \end{cases} \quad (3)$$

where $\theta = (N, C, a)$ with $N, C, a \geq 0$ is the parameter vector to be estimated. h can be $\boldsymbol{h}_s$ or h_t. In the exponential model, a is called the range, where the variogram value stabilized at a value, C is the partial sill. N is called nugget effect, it is the semivariance when spatial lag h is close to 0.

In this study, three nonseparable models, including the product-sum model [12], [27], Cressie–Huang model [20], and Gneiting model [18] are investigated. Their analytical expressions are given below.

1) Product-Sum Model: In this study, the product-sum model, with exponential marginal variograms (without marginal nugget) and a global nugget effect [12], is used and given by

$$\gamma(\boldsymbol{h}_s, h_t; \theta_p)$$
$$= \begin{cases} 0, & (\boldsymbol{h}_s, h_t) = (\boldsymbol{0}, 0) \\ N_{ST} + C_S \cdot (1 - \exp(-\|\boldsymbol{h}_s\|/a)) \\ \quad + C_T \cdot (1 - \exp(-|h_t|/b)) \\ \quad - k \cdot (C_S \cdot (1 - \exp(-\|\boldsymbol{h}_s\|/a))) \\ \quad \cdot (C_T \cdot (1 - \exp(-|h_t|/b))) & \text{otherwise} \end{cases}$$
$$(4)$$

where $\theta_p = (N_{ST}, C_S, a, C_T, b, k)$ is the parameter vector to be estimated, with $N_{ST}, C_S, a, C_T, b \geq 0$ and $0 < k \leq 1/\max\{C_S, C_T\}$ [27]. The parameters are estimated simultaneously using the same approach as in [21], to overcome the limitations of the fitting by marginal variogram procedure used in [32].

2) Cressie–Huang Model:

$$\gamma(\boldsymbol{h}_s, h_t; \theta_c)$$
$$= \begin{cases} 0, & (\boldsymbol{h}_s, h_t) = (\boldsymbol{0}, 0) \\ N_{ST} + C_{ST} \cdot (1 - \exp(-\|\boldsymbol{h}_s\|/a)) \\ \quad \cdot \exp((-\|\boldsymbol{h}_s\|/a) \cdot \exp(-|h_t|/b)), & \text{otherwise} \end{cases}$$
$$(5)$$

where $\theta_c = (N_{ST}, C_{ST}, a, b)$, with $N_{ST}, C_{ST}, a, b \geq 0$, is the parameter vector to be estimated.

3) Gneiting Model:

$$\gamma(\boldsymbol{h}_s, h_t; \theta_g)$$
$$= \begin{cases} 0, & (\boldsymbol{h}_s, h_t) = (\boldsymbol{0}, 0) \\ N_{ST} + C_{ST} \cdot (1 - \exp(-|h_t|/b))^\tau \\ \quad \cdot \exp\left((-\|\boldsymbol{h}_s\|/a) \cdot \exp(-|h_t|/b)^\beta\right), & \text{otherwise} \end{cases}$$
$$(6)$$

where $\theta_c = (N_{ST}, C_{ST}, a, b, \tau, \beta)$, with $N_{ST}, C_{ST}, a, b \geq 0$, $\beta \in [0, 1], \tau \geq \beta$ is the parameter vector to be estimated.

The nonlinear weighted least-squared technique [10], [17], [40] is used to estimate the parameters in the above spatio-temporal variogram models in this study. This procedure gives an estimate for the parameters over all the values, by minimizing the following weighted sum

$$W(\theta) = \sum_{I(r_s, r_t)} |I(r_s, r_t)| \cdot \left[\frac{\hat{\gamma}(\overline{h_s}, \overline{h_t})}{\gamma(\overline{h_s}, \overline{h_t}; \theta)} - 1 \right]^2 \quad (7)$$

where $I(r_s, r_t)$ has been described in (2), and $\overline{h_s}$ and $\overline{h_t}$ are the average distances that fall, respectively, in the tolerance region around r_s and r_t such that $\|r_s - h_s\| < \delta_s$ and $\|r_t - h_t\| < \delta_t\}$. The minimized sum $W(\theta)$, namely WMSE, measures the performance of fitting the variogram models to the empirical variogram surface. The smaller the $W(\theta)$ is, the better the fitting will be.

D. Spatio-Temporal Geostatistical Prediction

The space–time ordinary kriging [23], [39], which is a commonly used geostatistical prediction method, is used to predict the value $R(s_0, t_0)$, at unsampled location (s_0, t_0), from the stochastic residual component $R = R(s, t), (s, t) \in D \times T$. The prediction method predicts $R^*(s_0, t_0)$ as a linear combination of residual data local in space and time to the prediction location (s_0, t_0). Suppose that $R^*(s_0, t_0)$ is a prediction of $R(s_0, t_0)$ and the local data number is $n(s_0, t_0)$, which will be defined below, then

$$R^*(s_0, t_0) = \sum_{i=1}^{n(s_0, t_0)} \lambda_i(s_0, t_0) R(s_i, t_i),$$

$$\text{with} \sum_{i=1}^{n(s_0, t_0)} \lambda_i(s_0, t_0) = 1. \quad (8)$$

The weight λ assigning to each neighboring datum is quantified so as to minimize the mean-squared prediction error $\mathrm{E}(R(s_0, t_0) - R^*(s_0, t_0))^2$, while maintaining unbiasedness of the predictor $R^*(s_0, t_0)$. The minimized mean-squared prediction error is called the kriging variance [10], which is a measurement of prediction uncertainty [41], [42]. In determining the optimum weight λ, kriging takes both the variances between R and $R(s_0, t_0)$, and the variances of the data R itself into account, in which the variances value is derived from the fitted spatio-temporal variogram model in (4)–(6).

During the prediction process using spatio-temporal kriging, the kriging neighborhood recommended by Zeng *et al.* [12] will be used in order to make it computationally practical and preserve the local variability of X_{CO_2}. Assume that the location (s_0, t_0) is the datum to be predicted, the prediction procedure can be briefly summarized as follows. First, the kriging neighborhood is defined by setting the initial search range to 300 km in space and 20 time units, and if the number of points within the search range is less than 20, then the neighborhood will expand until the number is larger than 20 while the radii of the search range do not exceed the limits, which are set to 500 km in

space and 40 time units in time. Second, the residual at (s_0, t_0), denoted as $R^*(s_0, t_0)$, is predicted using the space–time kriging described above. Finally, the predicted X_{CO_2} denoted as $Z^*(s_0, t_0)$ at the location (s_0, t_0) is obtained by adding the spatio-temporal trend $m(s_0, t_0)$ to the $R^*(s_0, t_0)$.

E. Evaluation of Prediction Accuracies

Cross-validation [10], [17], [43] is adopted to compare the performance of the three spatio-temporal variogram models fitted to the data. Throughout the cross-validation procedure, the full ACOS-GOSAT dataset in mainland China, denoted as $\{Z(s_i, t_i) : i = 1, \ldots, n\}$ $(n = 23\,120)$, is used to generate the prediction dataset $\{Z^*(s_i, t_i) : i = 1, \ldots, n\}$, obtained by using spatio-temporal geostatistical prediction on the basis of the above three variogram models. The leave-one-out cross-validation [10] is implemented in the following repeating calculation procedure. For each calculation, the datum $Z(s_j, t_j)$ is excluded from the full dataset and then is predicted with the neighboring data points choosing from the remaining dataset $\{Z(s_i, t_i) : i = 1, \ldots, j-1, j+1, \ldots, n\}$ $(n = 23\,120)$ [10]. Using the prediction and the original dataset, we calculate seven summary statistics [12], [23], [43] in cross-validation, including the correlation coefficients (CORR), the mean absolute prediction errors (MAPE), the slope of regression (SR), the intercept of regression (IR), the mean prediction errors (MPE), the variance of prediction errors (VPE), and the percentage of prediction error (PPE) within 2and 1 ppm, to assess the different spatio-temporal kriging prediction accuracies with the three fitted models. As shown in Houweling *et al.* [44], the highest precision of 1 ppm of the global X_{CO_2} data would best address the largest number of carbon science questions; Miller *et al.* [45] estimate that the precision of 1–2 ppm is necessary to monitor carbon fluxes at regional scales. Therefore, both the statistics of the PPE within 1 and 2 ppm will be important for further analysis of the mapping dataset.

IV. RESULTS AND DISCUSSION

A. Trend Analysis

Fig. 2(a) and (b) shows the GOSAT X_{CO_2} values along longitude and latitude directions, respectively, and Fig. 2(c) shows the same data in three-dimensional (3-D) perspective. Exploratory analysis by fitting the data using second-order polynomial shows that, the study area presents a minor decrease trend along the latitude, and along the longitude, the trend values in both sides are slightly higher than that in the middle. We found the spatial distribution of X_{CO_2} over the study area presents a spatial trend that varies generally with the latitudinal and longitudinal gradient. Therefore, we modeled the large-scale spatial structure model of X_{CO_2} using a full second-order polynomial trend surface, given by

$$p(x, y) = p_{00} + p_{10}x + p_{01}y + p_{20}x^2 + p_{11}xy + p_{02}y^2 \quad (9)$$

where x is the latitude value and y is the longitude value of the GOSAT data. p is the parameter vector to be estimated. As a result, the parameter vector estimation is $p = (p_{00} = 397.900, p_{10} = 0.028, p_{01} = -0.178, p_{20} = 2.714 \times 10^{-5}$,
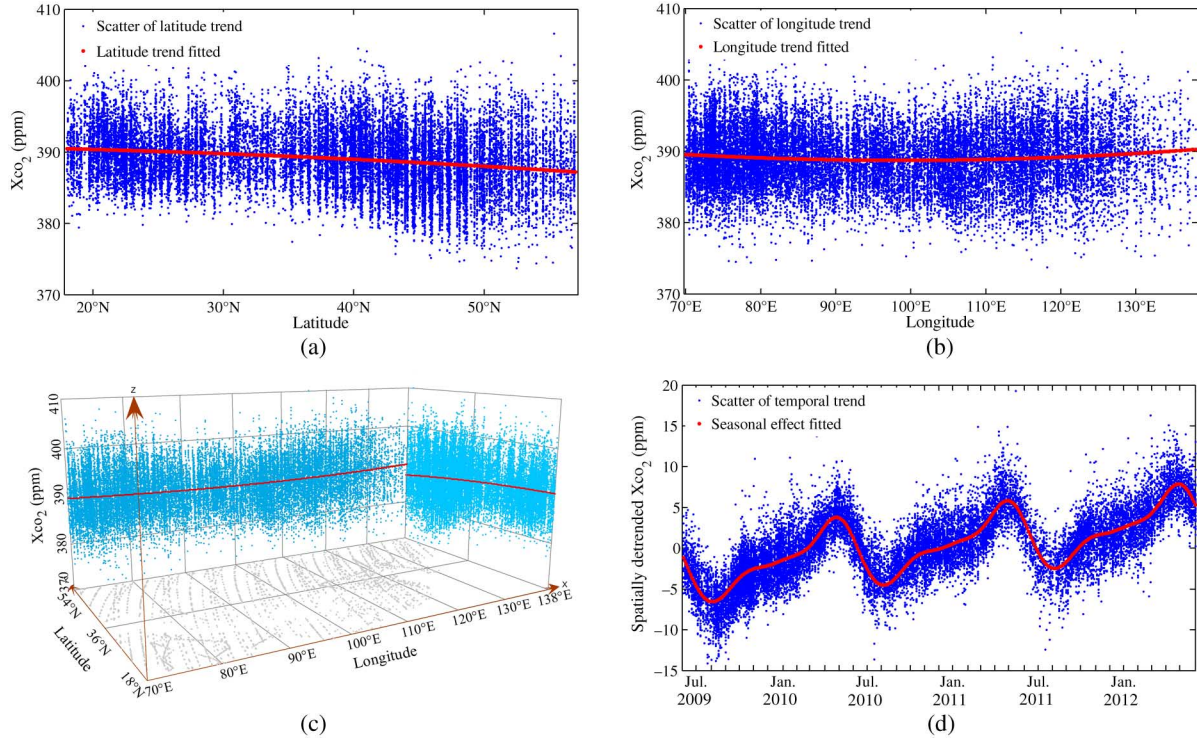
Fig. 2. Distribution of ACOS-GOSAT Xco_2 data (blue dots) along (a) latitude direction and (b) longitude direction, and their corresponding fitted trend (red line) using second-order polynomial function over the study area; (c) the spatial and temporal trend (red lines) shown in 3-D perspective; and (d) the time series of spatial-trend removed ACOS-GOSAT Xco_2 data (blue dots) over the study area and fitted temporal trend (red line).

$p_{11} = -0.001$, $p_{02} = 0.001$). Moreover, Fig. 2(d) shows the time series of the GOSAT Xco_2 data in which the modeled spatial trend is excluded. It can be indicated from Fig. 2(d) that the temporal variation of spatial trend removed GOSAT Xco_2 presents a strong seasonal effect, which is in agreement with the description in [13]. A combination of annual harmonic functions is used to model the temporal trend, as described in [12] and [13]. The used annual harmonic functions is given by

$$m_2(t) = a_0 + a_1 t + \sum_{i=1}^{4} \left(\alpha_i \sin(i\omega t) + \beta_i \cos(i\omega t) \right) \quad (10)$$

where $\omega = 2\pi/T$, and T is the period. The parameters are estimated using least squared techniques and the results are: $a_0 = -3.049$, $a_1 = 0.017$, $\alpha_1 = -0.727$, $\beta_1 = 2.945$, $\alpha_2 = 1.538$, $\beta_2 = 1.091$, $\alpha_3 = 0.425$, $\beta_3 = -0.261$, $\alpha_4 0.103$, $\beta_4 = 0.014$. The spatio-temporal trend is then subtracted from the full ACOS v3.3 mainland China dataset to yield the ACOS v3.3 Xco_2 residual dataset $R(s, t)$, an intrinsically stationary spatio-temporal error process used in the following section.

B. Variograms

Fig. 3 shows the empirical spatial and temporal marginal variograms, which are convex in both $\|h_s\|$ and $|h_t|$ for small spatial and temporal lags. It is reasonable to fit the empirical variograms with the commonly used exponential variogram model, which is applicable for convex variogram [30]. As a result, the estimated parameters in (3) are ($N_S = 1.674$, $C_S = 3.978$, $a_s = 1594.407$) for spatial marginal variogram and

($N_T = 1.666$, $C_T = 5.987$, $a_T = 71.606$) for the temporal marginal variogram. The corresponding optimal fitted variogram models are illustrated in Fig. 3, from which significant spatial and temporal correlation in the Xco_2 observations can be identified, because the ratio, $N/(N + C)$, is less than 0.75 for both the spatial and temporal cases.

As indicated in Fig. 3, the empirical variograms and the fitted variogram modeling using exponential model show a good agreement. We further model the empirical spatio-temporal variogram using the product-sum, Cressie–Huang, and Gneiting models in (4), (5), and (6) with exponential marginal structure. We can see that the two margins behave differently at infinity. It is worth highlighting, as specified in [32], that the product-sum model in (4) can naturally catch this characteristic, while the Gneiting model constructed as in (6) does not have this feature [32].

Fig. 4 shows the empirical spatio-temporal variogram of the residual component and the corresponding fitted variogram models using the product-sum, Cressie–Huang, and Gneiting models, respectively. Table I shows the estimated parameters and the WMSE of the fitting.

As indicated from the results of $W(\theta)$ given in Table I, the difference between the three variogram models is small. As a result, both the product-sum model and Gneiting model present a slightly better fit than Cressie–Huang model, which has the largest $W(\theta)$. The fit near the origin (N_{ST}) of the product-sum model is 1.695, while for Cressie–Huang model and Gneiting model, they are 1.731 and 1.699, respectively. From the calculations of empirical spatio-temporal variogram, as shown in Fig. 4(a), the empirical value at the origin should
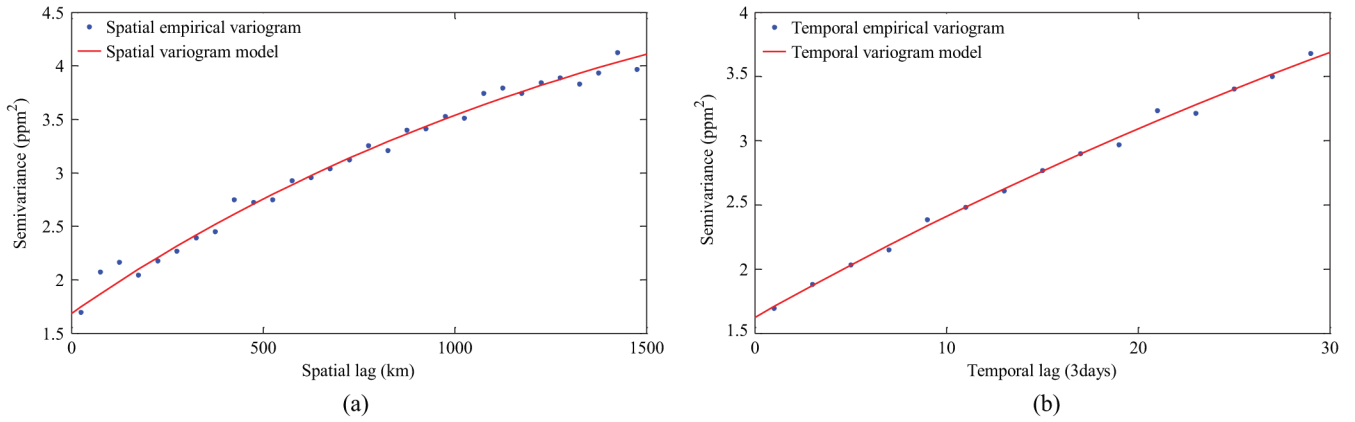
Fig. 3. Marginal (a) spatial and (b) temporal empirical variogram of ACOS-GOSAT Xco₂ residuals over the study area, and the corresponding fitted marginal variogram models.
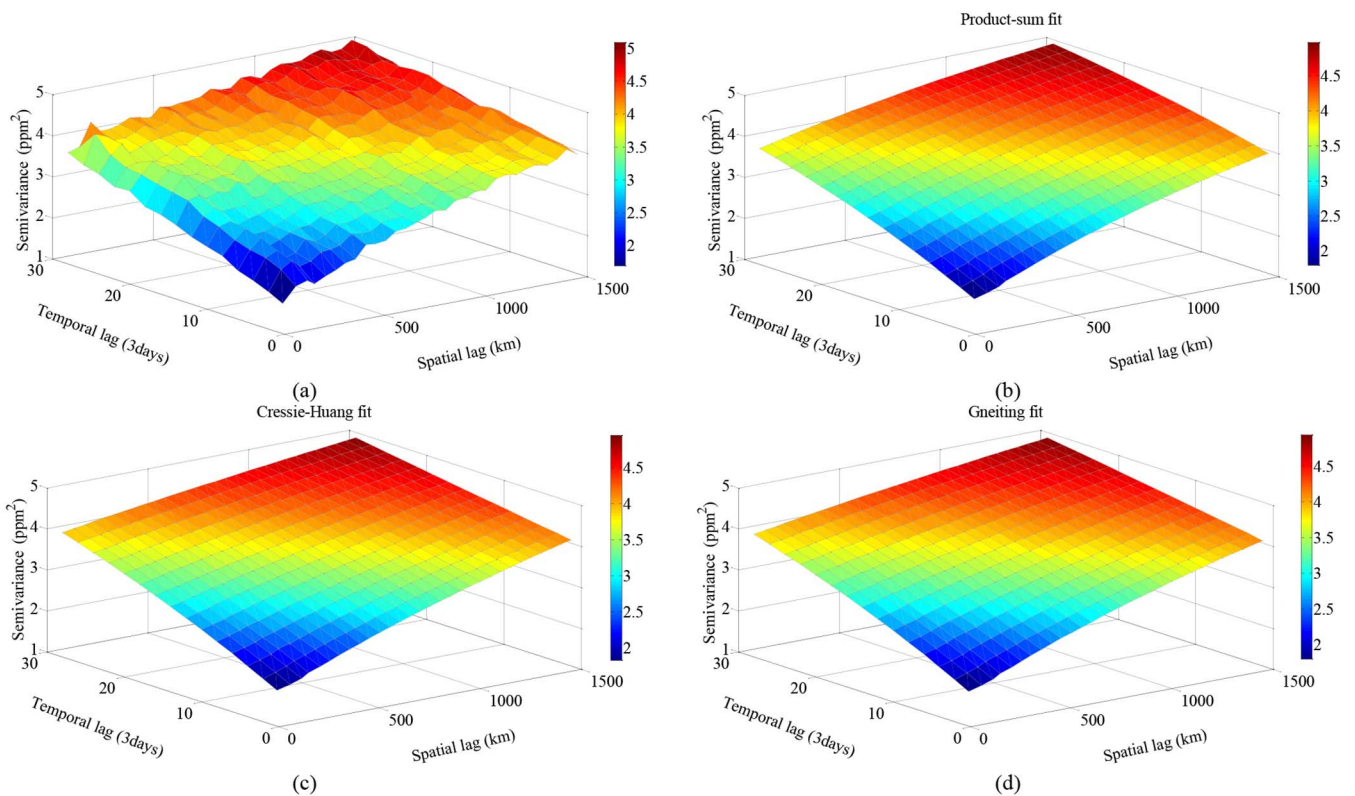

Fig. 4. (a) Spatio-temporal empirical variogram and (b) the three fitted spatio-temporal variogram models using the product-sum model; (c) Cressie–Huang model; and (d) Gneiting model.

be slightly lower than the sample variogram at the first spatio-temporal lag, $\hat{\gamma}_{ST}(50\,\text{km}, 3\,\text{days})$, which is 1.695. Therefore, the product-sum model well fit the variogram value near the origin and is slightly better than the other two models in the fitness near the origin. Because kriging is carried out in local neighborhood and data closer to the prediction location will have more substantial weights, the fitting of variogram at small lags is therefore important in prediction and mapping [10].

C. Evaluation for Prediction Precision of Different Variogram Models

In Table II, some descriptive statistics computed on cross-validation results are given. Note that all the three models

present similar summary statistics in cross-validation. All of them present significantly high correlation coefficient (CORR) of 0.92 which indicates high correlation between the original dataset and the prediction dataset. Their MPE are all 0.005, and the PPE within 2 ppm is about 83% and within 1 ppm is about 53% in the cross-validation results. The product-sum model has a slightly better performance in terms of MAPE, VPE, and PPE. As a conclusion from the results of Table II, all the three models can precisely catch the empirical characteristics of the spatio-temporal correlation structure of Xco₂ in China, and therefore the precision and effectiveness of predicting and mapping Xco₂ using the three models are almost the same.

TABLE I
PARAMETERS ESTIMATES FOR PRODUCT-SUM, CRESSIE–HUANG, AND GNEITING MODELS AND CORRESPONDING
WMSE, DENOTED AS $W(\theta)$

Product-sum model	$\theta_p = (N_{ST} = 1.695, C_S = 4.000, a = 1751.325, C_T = 4.133, b = 41.217, k = 0.226);$ $W(\theta) = 7100$
Cressie–Huang model	$\theta_c = (N_{ST} = 1.731, C_{ST} = 5.633, a = 2651.923, b = 0.018);$ $W(\theta) = 7263$
Gneiting model	$\theta_p = (N_{ST} = 1.699, C_{ST} = 5.101, a = 4.344 \times 10^{-4}, b = 0.0438, \tau = 0.463, \beta = 0.320);$ $W(\theta) = 7091$

TABLE II
SUMMARY STATISTICS FROM CROSS-VALIDATION, INCLUDING CORR, MAPE, MPE, VPE, SR, IRS, AND PPE WITHIN 2 PPM
AND WITHIN 1 PPM FOR PRODUCT-SUM, CRESSIE–HUANG, AND GNEITING MODELS

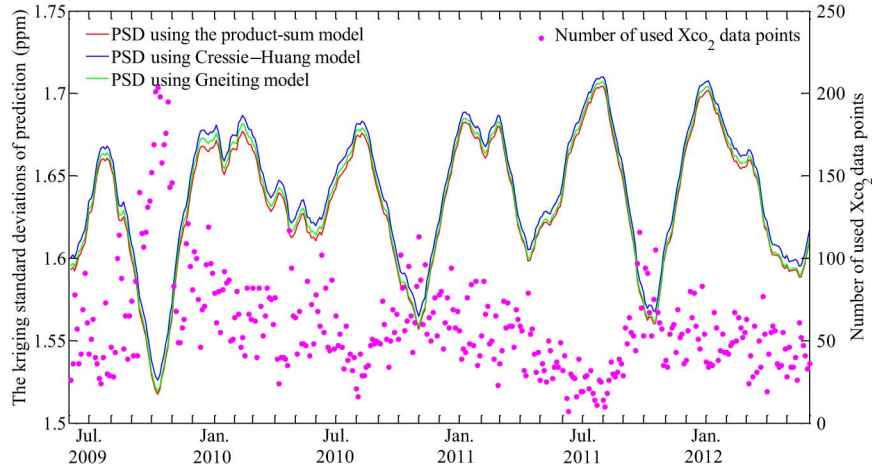|	CORR	MAPE (ppm)	MPE (ppm)	VPE	SR	IR	PPE (%)	
							2 ppm	1 ppm
Product-sum model	0.922	1.186	0.005	2.506	1.006	-2.411	83.11	52.93
Cressie–Huang model	0.921	1.190	0.005	2.519	1.007	-2.506	82.99	52.84
Gneiting model	0.922	1.188	0.005	2.512	1.006	-2.370	83.09	52.90

Fig. 5. Temporal variation of the averaged kriging standard deviations of prediction (PSD) using product-sum, Cressie–Huang, and Gneiting models for the whole of the study area from June 2009 to May 2012, and the temporal variation of the number of used original Xco_2 data points (purple dots).

TABLE III
MEAN VALUE OF TEMPORALLY AVERAGED KRIGING PREDICTION
STANDARD DEVIATION

Product-sum model	Cressie–Huang model	Gneiting model
1.633	1.641	1.636

D. Performance of Models in Mapping Xco_2

The study area is divided into $1° \times 1°$ regular grids, Xco_2 value at the center of each grid box is predicted in 3-day interval using the spatio-temporal kriging with the above three fitted variogram models using the full dataset of ACOS-GOSAT data to generate the gap-filled maps of Xco_2. The kriging standard deviation (root kriging variance) is also calculated to quantify the prediction uncertainty corresponding to the Xco_2 mapping results.

Fig. 5 shows the temporal variation of kriging standard deviations, which are averaged for the whole study area from June 2009 to May 2012, using the predictions with product-sum, Cressie–Huang, and Gneiting variogram models, and also shows the number of Xco_2 observations used within each time unit. It can be seen from Fig. 5 that the prediction uncertainty for the three variogram models presents almost the same temporal variation pattern and their differences of standard deviations are small. The maximum difference of standard deviations is about 0.010 between the product-sum model and Cressie–Huang model in December 2009, when the number of available Xco_2 data points is very limited. It can be found from Fig. 5 that the fewer number of used original Xco_2 data points, the greater the prediction standard deviation for all of three variogram models, which implies that the kriging standard deviation of prediction has a negative correlation with the number of used Xco_2 data points. As a result of mean prediction standard deviation shown in Table III, there are no significant differences between results from three variogram models, in which the minimum value is 1.633 from the product-sum model and the maximum value is 1.641 from Cressie–Huang model.

Fig. 6 shows the distribution of the averaged prediction standard deviations in August 2010 when the number of used Xco_2 data points is relatively few. The averaged prediction standard deviations are calculated by averaging the kriging standard
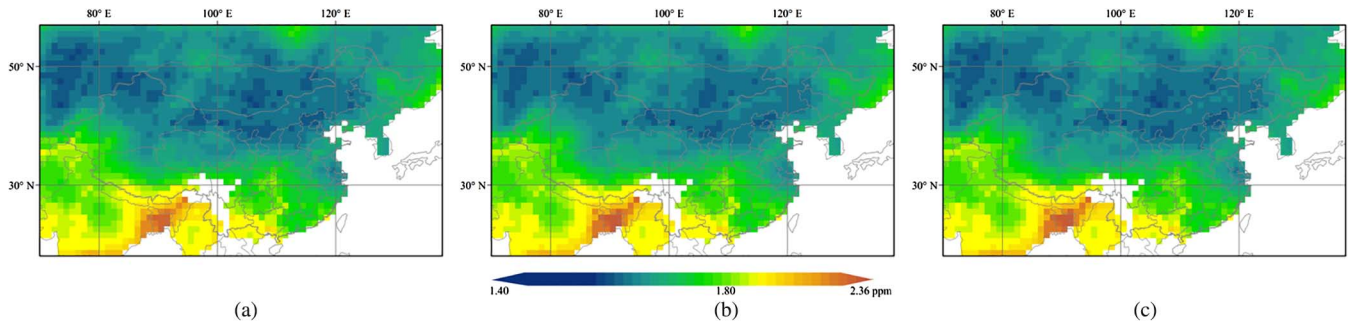
Fig. 6. Distribution of the averaged prediction standard deviations in August 2010, which is obtained by averaging the kriging standard deviation at all the grids in the study area over all time units (3-day interval) within August 2010, using (a) the product-sum model; (b) Cressie–Huang model; and (c) Gneiting model.
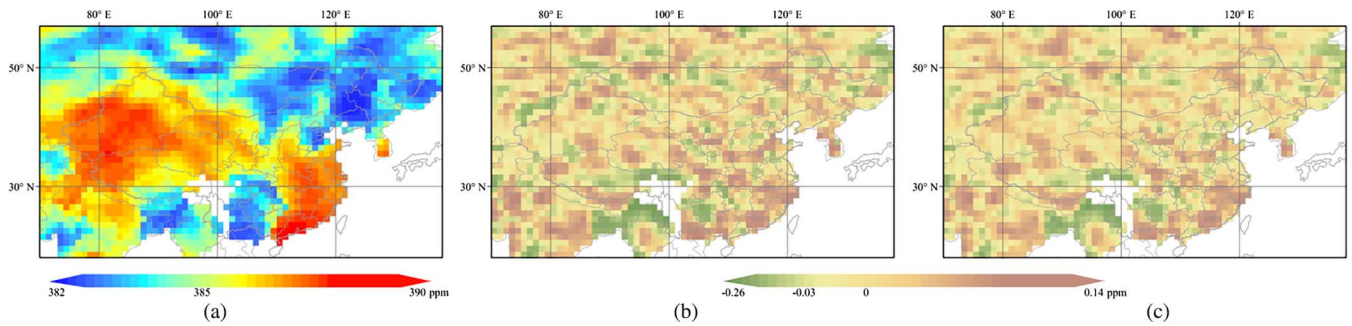

Fig. 7. (a) Map of averaged X_{CO_2} concentration in August 2010, which is derived by averaging all the time units (3-day interval) X_{CO_2} within August 2010 based on the kriging predictions with the product-sum model in $1° \times 1°$ grid. (b) shows the differences between the predicted X_{CO_2} with Cressie–Huang model and (a); (c) shows the differences between the predicted X_{CO_2} with Gneiting model and (a).

deviation value of each grid over all time units (3-day interval) within August 2010 for the three variogram models. From Fig. 6, it is shown that the spatial variations of the prediction standard deviations from the three variogram models are similar, and the prediction standard deviations for all models are generally lower in the northern region, where there are relatively more X_{CO_2} observations available than that in the southern region. This implication is in agreement with the results assessed using the model in the previous studies [46].

Fig. 7(a) presents the map of monthly averaged X_{CO_2} predicted using the product-sum model in August 2010, which is obtained by averaging the kriging predictions of all time units (3-day interval) within August 2010 for each grid, and Fig. 7(b) and (c) demonstrates the differences of monthly averaged X_{CO_2} predictions in August 2010 calculated by subtracting average X_{CO_2} predicted by the product-sum model from those predicted by Cressie–Huang model and Gneiting model, respectively. It can be seen from Fig. 7(b) and (c) that most of X_{CO_2} predicted by the product-sum model are slightly lower than those X_{CO_2} predicted by the other two models, but the differences between them are less than 0.26 ppm. On the other hand, X_{CO_2} predicted by the product-sum model is slightly larger than those X_{CO_2} predicted by the other two models with the differences from -0.03 to -0.26 ppm around the unpredicted blank areas shown in the south-western part of Chinese land where the less X_{CO_2} observations are available.

As the results show, the difference within the range $(-0.1, 0.1)$ accounts for more than 96%. When compared with the retrieval error, with mean bias of 1.34 ppm [37], of

ACOS-GOSAT data, the very small difference between the mapping results using the three models is not significant, and can therefore be ignored. The very small difference is largely due to the mapping using difference variogram models, since other kriging mapping processes are the same for the mapping results. Therefore, it can be concluded that no significant differences are identified for mapping X_{CO_2} using prediction with the three variogram models.

V. CONCLUSION

The objective of this study is focused on the evaluation of different well-known types of spatio-temporal nonseparable covariance functions, which are used to model the spatio-temporal correlation structure of data for kriging predictions and mapping of X_{CO_2} using satellite observations from ACOS-GOSAT. To begin with, the spatial trend and seasonal effect of X_{CO_2} in the study area over China are analyzed and then removed to obtain the residual component. The three typical spatio-temporal variogram models, the product-sum model, Cressie–Huang model, and Gneiting model, are then used to fit the empirical spatio-temporal variogram using a nonlinear weighted least square technique. The WMSE is used to measure the performance of fitting the variogram models to the empirical variogram surface. As a result, the model fitness of the product-sum model and Gneiting model is almost the same, and is slightly better than Cressie–Huang model, while the fitness near the origin with the product-sum model is slightly better than the other two models. Furthermore, the prediction

accuracies of spatio-temporal kriging with the three variogram models are assessed and compared using seven summary statistics of cross-validation results, including the CORR, the MAPE, the SR, the IR, the MPE, the VPE, and the PPE within 2 ppm. As a result, all the three models present similar summary statistics in cross-validation, all with a significantly high correlation coefficient of 0.92, and about 83% of predictions error within 2 ppm and about 53% within 1 ppm. Finally, performance of the three models when used to map Xco_2 in $1° \times 1°$ grid and 3-day temporal interval and corresponding prediction uncertainty is also discussed. It is found that the Xco_2 differences between the mapping results using the three models are generally less than 0.26 ppm, and no significant differences can be identified. As a conclusion from above results, all the three variogram models, namely the product-sum model, Cressie–Huang model, and Gneiting model, can precisely catch the empirical characteristics of the spatio-temporal correlation structure of Xco_2. We could obtain almost the same Xco_2 mapping results by the spatio-temporal kriging prediction using the three spatio-temporal variogram models when applied in China land region.

As regards computational aspects, though all the three variogram models present similar performance in modeling, prediction, and mapping, we found that the product-sum model, generated simply as a convex combination of spatial and temporal covariance [32], is relatively flexible and easy to implement. However, implementation of the fitting process of Cressie–Huang and Gneiting models need an iterative parameter optimization technique as specified in [30]. Moreover, to construct an appropriate spatio-temporal variogram model, it is important to study the main features of the marginal spatial and temporal variograms, such as the behavior near the origin. In this study, the results indicate that the exponential model with a nugget effect, which is convex in both the spatial and temporal cases, performs well by examining the shapes of empirical spatial and temporal variograms. Therefore, exponential function is specified as the spatial and temporal structure for the three spatio-temporal variogram models, the product-sum model, Cressie–Huang model, and Gneiting model.

Future studies will contribute to extending this comparison to other regions to further verify the conclusions drawn in this study, and interpretation and further validation of the mapping results to understand the spatio-temporal distribution and variability of Xco_2 in China.

ACKNOWLEDGMENT

REFERENCES

[1] L. M. Laurenza *et al.*, "Comparison of column-averaged volume mixing ratios of carbon dioxide retrieved from IASIMETOP-A using KLIMA algorithm and TANSO-FTSGOSAT level 2 products," *IEEE J. Sel. Topics Appl. Earth Observ. Remote Sens. (JSTARS)*, vol. 7, no. 2, pp. 389–398, Feb. 2014.

[2] T. Yokota *et al.*, "Global concentrations of CO2 and CH4 Retrieved from GOSAT: First preliminary results, scientific online letters on the atmosphere," *Sola*, vol. 5, pp. 160–163, 2009, doi: 10.2151/sola.2009-041.

[3] S. Maksyutov *et al.*, "Regional CO2 flux estimates for 2009–2010 based on GOSAT and ground-based CO2 observations," *Atmos. Chem. Phys. Discuss.*, vol. 12, pp. 29235–29288, 2012.

[4] S. Basu *et al.*, "Global CO2 fluxes estimated from GOSAT retrievals of total column CO2 ," *Atmos. Chem. Phys.*, vol. 13, pp. 8695–8717, 2013.

[5] NIES GOSAT Project, *Global Greenhouse Gas Observation By Satellite: GOSAT Project, GOSAT Project*, Jun. 2013.

[6] G. Keppel-Aleks, P. O. Wennberg, C. W. O'Dell, and D. Wunch, "Towards constraints on fossil fuel emissions from total column carbon dioxide," *Atmos. Chem. Phys.*, vol. 13, pp. 4349–4357, 2013.

[7] NIES GOSAT Project, *NIES-GOSAT-PO-017, v1.0 Algorithm Theoretical Basis Document for GOSAT TANSO-FTS L3*, NIES GOSAT Project, NIES-GOSAT-PO-017, v1.0, Feb. 2011.

[8] Z. Zeng, L. Lei, S. Hou, and L. Li, "A spatio-temporal interpolation approach for the FTS SWIR product of XCO2 data from GOSAT," in *Proc. IEEE Int. Geosci. Remote Sens. Symp. (IGARSS)*, Munich, Germany, Jul. 22–27, 2012, pp. 852–855.

[9] Z. Zeng, L. Lei, L. Guo, L. Zhang, and B. Zhang, "Incorporating temporal variability to improve geostatistical analysis of satellite-observed CO2 in China," *Chin. Sci. Bull.*, vol. 58, pp. 1948–1954, Jun. 2013.

[10] N. Cressie, *Statistics for Spatial Data*. Hoboken, NJ, USA: Wiley, 1993.

[11] S. De Iaco and D. Posa, "Positive and negative non-separability for space–time covariance models," *J. Stat. Plann. Infer.*, vol. 143, pp. 378–391, 2013.

[12] Z. Zeng *et al.*, "A regional gap-filling method based on spatio-temporal variogram model of CO2 columns," *IEEE Trans. Geosci. Remote Sens.*, vol. 52, no. 6, pp. 3594–3603, Jun. 2014.

[13] World Meteorological Organization. *WMO WDCGG Data Summary. WMO WDCGG no. 36*, 2012.

[14] M. Tomosada, K. Kanefuji, Y. Matsumoto, and H. Tsubaki, "A prediction method of the global distribution map of CO2 column abundance retrieved from GOSAT observation derived from ordinary Kriging," in *Proc. ICROS-SICE Int. Joint Conf.*, Japan, Aug. 2009, pp. 4869–4873.

[15] M. Tomosada, K. Kanefuji, Y. Matsumoto, and H. Tsubaki, "Application of the spatial statistics to the retrieved CO2 column abundances derived from GOSAT data," in *Proc. 4th WSEAS Int. Conf. Remote Sens.*, Venice, Italy, Nov. 2008, pp. 67–73.

[16] Y. Liu, X. Wang, M. Guo, and H. Tani, "Mapping the FTS SWIR L2 product of XCO2 and XCH4 data from the GOSAT by the Kriging method—A case study in East Asia," *Int. J. Remote Sens.*, vol. 33, no. 10, pp. 3004–3025, May 2012.

[17] S. De Iaco, M. Palma, and D. Posa, "Prediction of particle pollution through spatio-temporal multivariate geostatistical analysis: Spatial special issue," *AStA Adv. Stat. Anal.*, vol. 97, pp. 133–150, 2013.

[18] T. Gneiting, "Nonseparable, stationary covariance functions for space–time data," *J. Amer. Stat. Assoc.*, vol. 97, pp. 590–600, 2002.

[19] T. Gneiting, M. G. Genton, and P. Guttorp, "Geostatistical space—time models, stationary, separability, and full symmetry," in *Statistical Methods for Spatio-Temporal Systems*, B. Finkenstädt, L. Held, and V. Isham, Eds. London, U.K.: Chapman and Hall, 2007, pp. 151–175.

[20] N. Cressies and H. C. Huang, "Classes of nonseparable, spatio-temporal stationary covariance function," *J. Amer. Stat. Assoc.*, vol. 94, pp. 1330–1339, 1999.

[21] G. Jost, G. B. M. Heuvelink, and A. Papritz, "Analysing the space-time distribution of soil water storage of a forest ecosystem using spatio-temporal kriging," *Geoderma*, vol. 128, pp. 258–273, Oct. 2005.

[22] J. O. Skøien and G. Blöschl, "Catchments as space-time filters—A joint spatio-temporal geostatistical analysis of runoff and precipitation," *Hydrol. Earth Syst. Sci.*, vol. 10, pp. 645–662, Sep. 2006.

[23] P. W. Gething *et al.*, "A local space-time kriging approach applied to a national," *Comput. Geosci.*, vol. 33, pp. 1337–1350, Oct. 2007.

[24] F. Martínez-Ruiz, J. Mateu, F. Montes, and E. Porcu, "Mortality risk assessment through stationary space-time covariance functions," *Stoch. Environ. Res. Risk Assess.*, vol. 24, pp. 519–526, 2010.

[25] P. C. Kyriakidis and A. G. Journel, "Geostatistical space-time models: A review," *Math. Geol.*, vol. 31, no. 6, pp. 651–684, 1999.

[26] C. Ma, "Spatio-temporal covariance functions generated by mixtures," *Math. Geol.*, vol. 34, no. 8, pp. 965–975, Nov. 2002.

[27] S. De Iaco, D. E. Myers, and D. Posa, "Space-time analysis using a general product-sum model," *Statist. Probab. Lett.*, vol. 52, pp. 21–28, 2001.

[28] A. Kolovos, G. Christakos, D. T. Hristopulos, and M. L. Serre, "Methods for generating non-separable spatiotemporal covariance models with potential environmental applications," *Adv. Water Resour.*, vol. 27, pp. 815–830, 2004.

[29] A. Rodrigues and P. J. Diggle, "A class of convolution-based models for spatio-temporal processes with non-separable covariance structure," *Scand. J. Statist.*, vol. 37, pp. 553–567, Dec. 2010.

[30] S. De Iaco, "Space–time correlation analysis: A comparative study," *J. Appl. Statist.*, vol. 37, no. 6, pp. 1027–1041, Jun. 2010.

[31] H. C. Huang, F. Martinez, J. Mateu, and F. Montes, "Model comparison and selection for stationary space-time models," *Comput. Statist. Data Anal.*, vol. 51, pp. 4577–4596, 2007.

[32] S. De Iaco, D. Posa, and D. E. Myers, "Characteristics of some classes of space-time covariance functions," *J. Stat. Plann. Infer.*, vol. 143, pp. 2002–2015, Nov. 2013.

[33] M. Inoue *et al.*, "Validation of XCO_2 derived from SWIR spectra of GOSAT TANSO-FTS with aircraft measurement data," *Atmos. Chem. Phys.*, vol. 13, pp. 9771–9788, 2013.

[34] D. Wunch *et al.*, "Calibration of the total carbon column observing network using aircraft profile data," *Atmos. Meas. Tech.*, vol. 3, pp. 1351–1362, 2010.

[35] C. W. O'Dell *et al.*, "The ACOS CO_2 retrieval algorithm—Part 1: Description and validation against synthetic observations," *Atmos. Meas. Tech.*, vol. 5, no. 1, pp. 99–121, Jan. 2012.

[36] D. Crisp *et al.*, "The ACOS CO_2 retrieval algorithm—Part II: Global XCO_2 data characterization," *Atmos. Meas. Tech.*, vol. 5, pp. 687–707, 2012.

[37] National Aeronautics and Space Administration (NASA), *ACOS Level 2 Standard Product Data User's Guide, v3.3*. Greenbelt, MD, USA: GES DISC, Jun. 2013.

[38] S. De Iaco and D. Posa, "Predicting spatio-temporal random field: Some computational aspects," *Comput. Geosci.*, vol. 41, pp. 12–24, 2012.

[39] N. Cressie and C. K. Wikle, *Statistics for Spatio-Temporal Data*. Hoboken, NJ, USA: Wiley, 2011.

[40] N. Cressie, "Fitting variogram models by weighted least-squares," *Math. Geol.*, vol. 17, no. 5, pp. 563–586, 1985.

[41] J.-P. Chilès and P. Delfiner, "Kriging," in *Geostatistics: Modeling Spatial Uncertainty*, 2nd ed. Hoboken, NJ, USA: Wiley, 2008, ch. 3, pp. 150–230.

[42] D. M. Hammerling, A. M. Michalak, and S. R. Kawa, "Mapping of CO_2 at high spatiotemporal resolution using satellite observations: Global distributions from OCO-2," *J. Geophys. Res.*, vol. 117, no. D6, pp. D06306-1–D06306-10, 2012.

[43] S. Arlot, "A survey of cross-validation procedures for model selection," *Statist. Surv.*, vol. 4, pp. 40–79, 2010.

[44] S. Houweling *et al.*, "Inverse modeling of CO_2 sources and sinks using satellite data: A synthetic inter-comparison of measurement techniques and their performance as a function of space and time," *Atmos. Chem. Phys.*, vol. 4, pp. 523–538, 2004, doi: 10.5194/acp-4-523-2004.

[45] C. E. Miller *et al.*, "Precision requirements for space-based XCO_2 data," *J. Geophys. Res.*, vol. 112, p. D10314, 2007, doi: 10.1029/2006 JD007659.

[46] A. A. Alkhaled, A. M. Michalak, and S. R. Kawa, "Using CO_2 spatial variability to quantify representation errors of satellite CO_2 retrievals," *Geophys. Res. Lett.*, vol. 35, no. 16, pp. L16813-1–L16813-5, Aug. 2008.
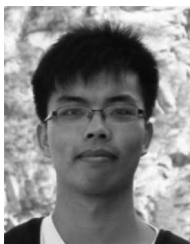
Lijie Guo received the B.S. degree in information and computing science from China University of Mining and Technology, Beijing, China, in 2012. She is currently pursuing the M.S. degree in cartography and geographic information system at the Institute of Remote Sensing and Digital Earth, Chinese Academy of Sciences, Beijing, China.

Her research interests include the CO_2 mapping by using satellite observations.

Liping Lei received the M.Sc. and B.A. degrees from Peking University, Beijing, China, in 1983 and 1986, respectively, and the Ph.D. degree in computer and information science from the Graduate School of Engineering, Iwate University, Morioka, Japan, in 1999.

She is currently a Professor with the Institute of Remote Sensing and Digital Earth, Chinese Academy of Sciences (CAS), Beijing, China. She was a Senior Researcher with the Basic Engineering Co. Ltd., Japan from 2003 to 2007 and worked as an Assistant Researcher with Iwate University from 1999 to 2002. She served as a Researcher with the Chinese Remote Sensing Satellite Receiving Station, CAS from 1986 to 1994. Her research interests include the greenhouse gases of remote sensing and developing time-series model for satellite observed data.

Zhao-Cheng Zeng received the B.S. degree with a double major in geoinformation and applied mathematics from Sun Yat-sen University, Guangzhou, China, in 2010, and the M.S. degree in cartography and geographic information system from the Institute of Remote Sensing and Digital Earth, Chinese Academy of Sciences, Beijing, China, in 2013. He is currently pursuing the Ph.D. degree in earth system and geoinformation science at the Institute of Space and Earth Information Science, The Chinese University of Hong Kong, Hong Kong.

His research interests include modeling the spatio-temporal dynamics of greenhouse gases in China using satellite observations.
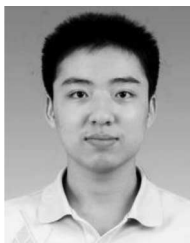
Pengfei Zou received the B.S. degree in remote sensing science and technology from the School of Remote Sensing and Information Engineering, Wuhan University, Wuhan, China, in 2012. He is currently pursuing the M.S. degree in cartography and geographic information system at the Institute of Remote Sensing and Digital Earth, Chinese Academy of Sciences, Beijing, China, in 2015.

His research interests include remote sensing image processing and SAR image segmentation.

Da Liu received the B.S. degree in remote sensing science and technology from the School of Remote Sensing and Information Engineering, Wuhan University, Wuhan, China, in 2010, and the M.S. degree in polarimetric SAR for agriculture and ocean from the School of Information Engineering, China University of Geosciences, Beijing, China, in 2013. He has been a Ph.D. candidate at the Institute of Remote Sensing and Digital Earth, Chinese Academy of Sciences, Beijing, China, since 2013.

His research interests include remote sensing information processing and its application on greenhouse gases.

Bing Zhang (M'11–SM'12) received the B.S. degree in geography from Peking University, Beijing, China, and the M.S. and Ph.D. degrees in remote sensing from the Institute of Remote Sensing Applications, Chinese Academy of Sciences (CAS), Beijing, China.

He is currently a Professor and the Deputy Director of the Institute of Remote Sensing and Digital Earth, CAS. He specializes in hyperspectral remote sensing and has more than 19 years of experience in studying and graduate education in this field. He is the author or coauthor of around 150 publications, including 100 journal citation papers and more than 50 peer-reviewed international conference papers. He has written four books on hyperspectral remote sensing, including *Hyper-Spectral Remote Sensing Hyper-Spectral Image Classification and Target Detection, Hyperspectral Remote Sensing for Inland Water*, and *Hyper-Spectral Remote Sensing and its Multidisciplinary Application*s. His research interests include development of physics-based models and image processing software for the use of hyperspectral remote sensing data in solving problems in geology, hydrology, ecology, and botany.

Dr. Zhang received several Chinese National, Ministerial, and Provincial S&T progress awards because of some remarkable innovative research and research-based development projects undertaken by him.